Interface structure of epitaxial graphene grown on 4H-SiC(0001)

J. Hass, J. E. Millán-Otoya, P. N. First, and E. H. Conrad
School of Physics, Georgia Institute of Technology, Atlanta, Georgia 30332-0430, USA
(Received 7 August 2008; revised manuscript received 16 October 2008; published 19 November 2008)

We present a structural analysis of the graphene-4HSiC(0001) interface using surface x-ray reflectivity. We find that the interface is composed of an extended reconstruction of two SiC bilayers. The interface directly below the first graphene sheet is an extended layer that is more than twice the thickness of a bulk SiC bilayer (~1.7 Å compared to 0.63 Å). The distance from this interface layer to the first graphene sheet is much smaller than the graphite interlayer spacing but larger than the same distance measured for graphene grown on the $(000\bar{1})$ surface, as predicted previously by *ab initio* calculations.

DOI: 10.1103/PhysRevB.78.205424 PACS number(s): 68.55.−a, 68.35.−p, 61.05.cp, 61.46.−w

I. INTRODUCTION

The direct growth of single or multiple sheets of graphene on an insulating or semiconducting substrate is known as epitaxial graphene (EG). Because this material has been identified as a viable all-carbon candidate for post complementary metal-oxide semiconductor (CMOS) electronics,[1] there is a strong impetus for the study of EG and how it can be produced, lithographically patterned, and made into electronic devices.[2–6] The current substrate for EG growth is either of the two polar faces of hexagonal SiC: the SiC(0001) Si-terminated surface (Si face) or the SiC$(000\bar{1})$ C-terminated surface (C-face). Multilayer epitaxial graphene films grown on C-face SiC show electronic properties expected for an isolated graphene sheet including a Berry's phase of π, weak antilocalization, and a square-root dependence of the Landau-level energies with applied magnetic field.[3,4,7–9] The fact that transport in graphene grown on SiC substrates is so similar to transport properties expected for an isolated graphene sheet is quite remarkable since graphene-substrate interactions and multilayer graphene stacking should potentially influence the two-dimensional (2D) Dirac electrons responsible for the unusual properties of graphene. On the other hand, these findings are very fortuitous and have made graphene grown on SiC the focus of research targeting a path toward graphene electronics.

Studies of the graphene/SiC interface substrate and multilayer graphene stacking have begun to elucidate the relationship between the electronic properties of EG and its structure. From the earliest measurements, it is clear that both the growth kinetics and consequent structure are very different for graphene grown on Si-face or C-face silicon carbide.[5,10–14] This is illustrated in Table I where we compare the properties of Si-face and C-face graphene grown in ultrahigh vacuum (UHV) and in higher-pressure furnace environments (for a review, see Ref. 15). Regardless of the growth environment, Si-face graphene is epitaxial with $(6\sqrt{3}\times 6\sqrt{3})$R30 periodicity as observed by low-energy electron diffraction (LEED) (i.e, the graphene is rotated 30° relative to the SiC $\langle 10\bar{1}0\rangle$ direction)[10,12] and grows in the normal graphitic *AB*… (Bernal) stacking.[19] C-face films, on the other hand, can have multiple orientational phases[10,14,16,20] with a complex rotational stacking order.[15,20] In addition graphene grows relatively slowly on the Si face compared with the C face.[11] This means that Si-face graphene films are typically ~1–4 layers thick, while graphene grown on the C-face grows rapidly compared to the Si face and can achieve thickness well above five layers.[5,12,13] Growth morphology has been a perpetual problem in UHV. Graphene grown on the C-face in UHV contains a high concentrations of graphene nanocaps[21] and other defects,[16] while graphene growth on the Si face causes the SiC substrate to roughen.[5] Huge improvements in graphene film morphology have been achieved by growing in high-pressure furnaces rather than in UHV.[15,17] As shown in Table I, both SiC substrate order and graphene film domain size have been improved by many orders of magnitude. It is important to note that despite improvements in film quality, the transport properties of Si-face films remain low[17] compared to C-face films[3,5,18] despite the rotational fault stacking of these films. Electron mobilities and electronic coherence lengths are several orders of magnitude higher on furnace-grown C-face graphene compared to either UHV or furnace-grown Si-face graphene.

For furnace-grown C-face films the high mobility is due to rotational stacking faults. It has been shown both experimentally[8,18] and theoretically[20,22,23] that the rotational faults electronically decouple adjacent layers by lifting the inequivalent interplaner interaction of *A* and *B* atoms in Bernal-stacked graphene. Why the mobility of Si-face films is comparatively so low, even with the improved furnace-grown films, is not known. It is possible that the interface plays a more important role in Si-face graphene simply because the *AB*… stacking requires a single graphene sheet to preserve the electronic properties of isolated graphene. The interaction of this single (or possibly two sheets) with the SiC substrate may have important consequences in its transport properties. For this reason, understanding the nature of the SiC(0001)/graphene interface is critical to understanding transport in Si-face graphene films.

Graphene grown on the Si-face of SiC has been the most extensively studied of the two hexagonal polar surfaces.[24–37] Despite this body of work, the structure of this interface is still unknown even though it is crucial for understanding the electronic structure of subsequent graphene layers and the charge transfer between the substrate and the graphene film. Early studies of the graphitization of the Si face presumed that the $(6\sqrt{3}\times 6\sqrt{3})$R30 pattern was due to the commensurate alignment of a graphene overlayer with an unrecon-

 ©2008 The American Physical Society

TABLE I. The structural and electronic properties of epitaxial graphene grown on Si-face SiC(0001) and C-face SiC(000$\bar{1}$) via heat treatment in UHV or in a low-vacuum furnace. The table compares the mean graphene domain size $\langle L_G \rangle$, minimum growth temperature T_{min}, number of graphene layers N, mean SiC terrace size $\langle L_{SiC} \rangle$, electron mobility μ, and the type of layer stacking. Values are compiled from Ref. 15 or from other sources as indicated.

	Surface	$\langle L_G \rangle$	T_{min} (°C)	N	$\langle L_{SiC} \rangle$	μ (cm^2/V s)	Stacking
	Si face	400–1000 Å	~1200	1–4	400–1000 Å [a]	<2000	*AB*...
UHV	C face	~500 Å [b]	~1100	1–10	~1000 Å		Rotational faults
	Si face	1–3 μm [c]	>1500 [c]	1–4[c]	~3 μm [c]	<2000 [c]	*AB*...
Furnace	C face	1–10 μm	>1250	5–50	~10 μm	>10^5 [d]	Rotational faults

[a]Substrate roughness increases at higher growth temperature.
[b]Reference 16.
[c]Reference 17.
[d]Reference 18.

structed SiC surface, forming a moiré pattern.[10,25–27] However, the consensus from recent experiments by many groups is that the $(6\sqrt{3}\times 6\sqrt{3})$R30 structure is a true structural precursor phase to graphene formation that persists, although slightly altered, after graphene has formed.[28–31,38] While scanning tunneling microscopy (STM) experiments have outlined some of the lateral features of the $(6\sqrt{3}\times 6\sqrt{3})$R30 structure,[24,29–31,39,40] the buried interface structure remains elusive.

In this paper, we use specular x-ray reflectivity to measure the buried structure of the graphene/4H-SiC(0001) interface. Because of the relative ease of growing graphene in UHV on SiC(0001) and the fact that mobilities do not improve in furnace-grown films, we have studied the structure of UHV-grown graphene on the Si face of SiC. We find that the first layer of carbon with an areal density of graphene sits close to the last layer of atoms in the interface layer. For the Si face the graphene-interface spacing is found to be 2.32 ± 0.08 Å. This number is consistent with *ab initio* calculations that predict a covalently bonded insulating first graphene layer that "buffers" subsequent graphene layers from the substrate.[41,42] However, unlike the simple bulk-terminated interface used in these calculations, the interface layer is found to be more complex. The structure of this interface layer suggests that it plays an important role in mediating the interaction of the SiC substrate with the graphene film.

II. EXPERIMENT

The substrates used in these studies were 4H-SiC purchased from Cree, Inc.[43] Prior to graphitization the $3\times 4\times 0.35$ mm^3 samples were ultrasonically cleaned in acetone and ethanol. The Si-face samples were H_2 etched[15] and subsequently graphitized in UHV ($P<1\times 10^{-10}$ Torr) by electron-bombardment heating. Substrates were first heated to 1100 °C for 6 min to form a $(\sqrt{3}\times\sqrt{3})$R30 reconstruction. After which they were heated to 1320 °C for 8 min to remove surface contamination and to form a well-ordered $(6\sqrt{3}\times 6\sqrt{3})$R30 reconstruction. The samples were subsequently heated to 1400–1440 °C for 6–12 min to create graphene films 1–3 layers thick. During graphitization the pressure in the system reached $P\lesssim 1\times 10^{-8}$ Torr. Despite the high pressure during growth, sample order is indistinguishable from Si-face sample order reported by other groups who grow the sample at pressures of $\sim 10^{-10}$ Torr or from those who use a Si flux to reduce surface oxides.[5,24,27,29,34] Growth-induced substrate roughening in all reported investigations of Si-face graphitization leads to average SiC terrace sizes of ~300–500 Å (graphene order is actually bigger than the terrace size because graphene grows over the SiC steps[35]). It appears that the long-range order of UHV-grown graphene on the Si face is not very sensitive to most details of the surface preparation.

Once the samples were graphitized, they remained inert allowing them to be transported into the separate x-ray scattering chamber for analysis. The x-ray scattering experiments were performed at the Advanced Photon Source, Argonne National Laboratory, on the 6IDC-μCAT UHV ($P<2\times 10^{-10}$ Torr) beam line. Experiments were performed at a photon energy of 16.2 keV. The number of graphene layers on the sample was determined by both Auger-electron spectroscopy (AES) and x-ray reflectivity (as described in Sec. III). The reflectivity data is presented in standard SiC hexagonal reciprocal-lattice units (r.l.u.) (h,k,ℓ). These are defined by the momentum-transfer vector $\mathbf{q}=(h\mathbf{a}^*_{SiC},k\mathbf{b}^*_{SiC},\ell\mathbf{c}^*_{SiC})$, where $a^*_{SiC}=b^*_{SiC}=2\pi/(a_{SiC}\sqrt{3}/2)$ and $c^*_{SiC}=2\pi/c_{SiC}$) (a_{SiC}, b_{SiC}, and c_{SiC} are the standard 4H-SiC hexagonal lattice constants). The measured lattice constants were $a_{SiC}=3.079\pm 0.001$ Å and $c_{SiC}=10.081\pm 0.002$ Å and are within error bars of published values.[44] For reference the nominal hexagonal lattice constants for graphite are $a_G=2.4589$ Å and $c_G=6.708$ Å.[45]

III. RESULTS

To obtain detailed information about both the graphene films and the SiC-graphene interface, we have measured the surface x-ray specular reflectivity from graphitized 4H-SiC(0001). Details of the data collection and the model are similar to those used to determine the structure of the

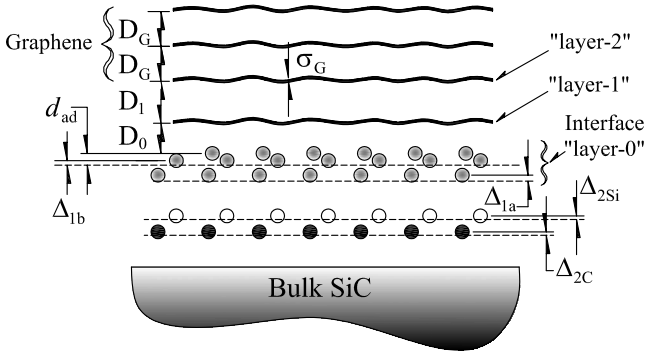

FIG. 1. Schematic model of multilayer graphene grown on the 4H-SiC(0001) substrate. Dashed lines are the bulk SiC lattice planes before interface relaxation (Δ's). The fifth plane of atoms (adatom) is displaced d_{ad} from the topmost atom plane in the interface. (●) is carbon atoms and (○) is silicon atoms. The shaded circles in the interface (layer-0) can be either carbon or silicon atoms. The graphene layers above the interface layer are referred to as layer-1, -2, -3, etc.

4H-SiC(000$\bar{1}$)/graphene system.[46] The data is collected by integrating rocking curves for different perpendicular momentum-transfer vectors $q_\perp = 2\pi\ell/c_{SiC}$, where $\mathbf{q}=\mathbf{k}_f-\mathbf{k}_i$. Since the reflectivity only depends on $q_\perp$ (or equivalently ℓ), the data can be analyzed using a one-dimensional model where all lateral information is averaged over the 0.4×0.4 mm^2 x-ray beam.

The schematic model of the graphene-covered SiC(0001) surface is shown in Fig. 1. This general model allows us to explore a number of possible graphene/SiC structures proposed by previous experiments. In the model the SiC substrate contribution is broken into two terms: (i) the amplitude from a bulk-terminated surface and (ii) the combined amplitude from a relaxed SiC bilayer just above the bulk and a reconstructed interface layer (defined as the interface "layer-"). The scattered x-ray intensity $I(\Theta,\ell)$ is then the result of a sum of three scattered amplitudes: the bulk F_{bulk}, the interface region F_I, and the graphene F_G

$$I(\Theta,\ell) = A(\Theta,\ell)e^{-4\gamma_{SiC}\sin^2 \pi\ell/2} \times \left| \frac{F_{bulk}(\ell)}{1-e^{-2\pi i\ell}} + F_I(\ell) + \frac{\rho_G}{\rho_{SiC}}F_G(\ell) \right|^2. \quad (1)$$

$A(\Theta,\ell)$ is a term that contains all corrections due to the experimental geometry.[47–49] The exponential term accounts for the substrate roughness caused by half-cell step fluctuations in the SiC surface (the predominant step height on 4H samples;[5] $c_{SiC}/2$). γ_{SiC} is the variance in the number of half-cell layers in the surface due to steps.[50] Roughly, γ_{SiC} is proportional to the SiC step density. The first term in Eq. (1) is the bulk 4H-SiC structure factor $F_{bulk}(\ell)$ (Ref. 51) modified by the crystal truncation term $(1-e^{-2\pi i\ell})^{-1}$ (Ref. 52). $F_G(\ell)$ in Eq. (1) is weighted by the ratio of the areal densities of a 4H-SiC(0001) and a graphene (0001) plane, $\rho_G/\rho_{Si} = 3.132$, to properly normalize the scattered amplitude from the graphene layer per 4H-SiC(0001) (1×1) unit cell.

$F_I(\ell)$ in Eq. (1) is the structure factor of the interface region between the bulk and the graphene film. Although we cannot obtain lateral information about the SiC(0001) $(6\sqrt{3}\times 6\sqrt{3})$R30 structure from reflectivity data, the vertical shifts of atoms and layer density changes associated with them can be determined. To begin to understand this interface, we allow for a reconstruction by placing a SiC bilayer plus an interface containing up to three additional atomic layers between the bulk and the multilayer graphene film (see Fig. 1). We then write the interface structure factor as

$$F_I(\ell) = \sum_{j=1}^{5} f_j(\ell)\rho_j e^{i2\pi\ell z_j/c_{SiC}}, \quad (2)$$

where ρ_j is the relative atom density for the jth interface layer ($\rho_j=1$ for a bulk layer corresponding to 8.22×10^{-16} atoms cm^{-2}) at a vertical position z_j (the zero height is chosen as the last layer of atoms in the interface). $f_j(\ell)$ is the atomic form factor of C or Si. The fifth atom layer is added to explore the possibility of adatoms between the SiC and the graphene.

To be completely general the scattered amplitude from the graphene film takes into account the possibility of a lateral distribution of varying graphene layers. This is done by defining an occupancy parameter p_n as the fractional surface area covered by all graphene islands that are n graphene layers thick. p_n is subjected to the constraint equation $\Sigma p_n = 1$, where p_0 is the fraction of area that has no graphene. The multilayer graphene structure factor can then be written in the general form

$$F_G(\ell) = f_C(\ell)\sum_{n=1}^{N_{max}} p_n \left\{ \sum_{m=1}^{n} F_m(\ell)e^{2\pi i l z_m/c_G} \right\}, \quad (3a)$$

$$z_m = \begin{cases} D_0 + (m-1)D_1 & m \le 2 \\ D_0 + D_1 + (m-2)D_G & m > 2 \end{cases}. \quad (3b)$$

f_C is the atomic form factor for carbon and N_{max} is the number of layers in the thickest graphene film on the surface. D_0 is the spacing between the bottom layer of an island and the last atom layer in the interface. D_1 is the spacing between graphene layer-1 and layer-2, while D_G is the average layer spacing between graphene in subsequent layers (see Fig. 1).

Because STM studies of multilayer graphene films grown on the Si face indicate some buckling of the graphite layer,[24,30,31] we must allow for a small vertical height distribution in each graphene layer that gives rise to a structure factor, $F_m(\ell)$ in Eq. (3a), for each layer. A vertical modulation of the graphene layers can be modeled in two ways. The simplest method is to assume an average layer-independent random vertical disorder σ_G that will give rise to a Debye-Waller term for each layer, i.e., $F_m(\ell)=e^{-q_\perp^2\sigma_G^2/2}$. Because the vertical modulation is known to decay quickly after the first graphene layer,[30] a more refined model uses the same average Debye-Waller term for the upper graphene layers but allows for a different distribution of carbon atoms in the first graphene layer such as those calculated in *ab initio* calculations.[53] In this case the structure factor of the first

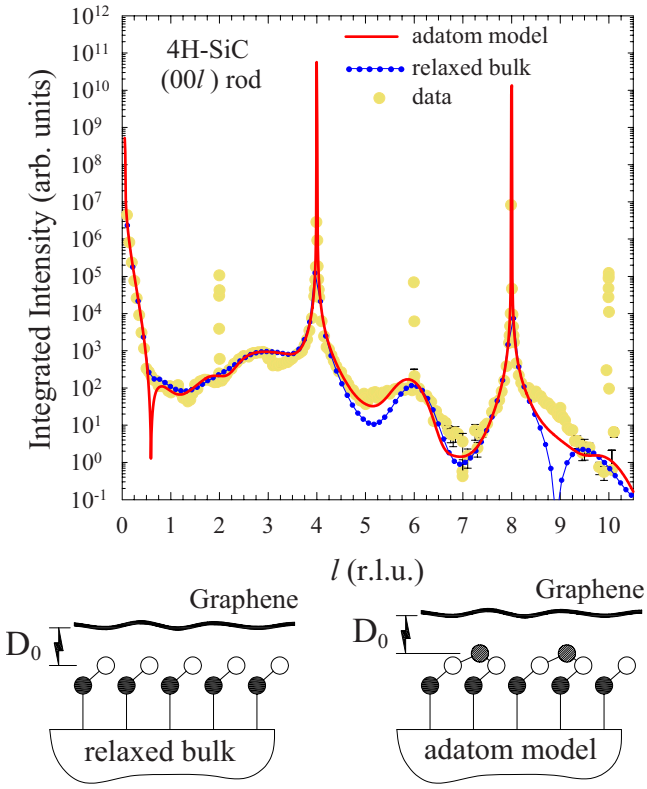

FIG. 2. (Color online) Specular reflectivity versus $q_\perp$ (in r.l.u.) for a graphitized 4H-SiC(0001) Si-face surface. Circles are the data. Fits to the two model structures in the figure are given. In the schematic models filled and open circles are C and Si atoms, respectively. Shaded circles are Si adatoms. Dotted blue line is a fit to a bulk-terminated SiC(0001) surface with a single relaxed bilayer. Solid red line is a fit to a model similar to the relaxed bilayer but with the addition of a layer of Si adatoms with $\rho_{ad}=0.21$.

layer $F_1(\ell)$ needs to be known. As we will show, both models give very similar results.

Reflectivity data for a Si-face multilayer graphene film are shown in Fig. 2. The main bulk 4H-SiC peaks occur at $\ell=4$ and 8. The sharp peaks at $\ell=2$, 6, and 10 are the "quasi-forbidden" reflections of bulk SiC.[51] In SiC reciprocal-lattice units, the graphite bulk reflections are nominally expected at $\ell\sim 3$, 6, and 9 [i.e., $\ell=\ell_G(c_{SiC}/c_G)$, where $\ell_G=0,2,4$, etc.].

We have tested a number of structural models for the graphene/4H-SiC(0001) interface. While the majority of experimental studies point to a complicated interface structure, simple models consisting of a nearly bulk-terminated substrate with the graphene on top are still being proposed.[54] However, such models always give poor fits to the x-ray data. This is demonstrated in Fig. 2 where we plot the best-fit reflectivity for a bulk-terminated surface where the $6\sqrt{3}$ interface layer is essentially a graphene layer as suggested by Emtsev *et al.*[54] In this model, the interface layer-0 in Fig. 1 is replaced by a single carbon layer with a graphitic density. The last bulk bilayer density is kept constant at the bulk value while the bilayer spacings are allowed to relax (the relaxation from the bulk value are small; $\Delta_{2C}=-0.03$ Å and $\Delta_{2Si}=0.01$ Å). All other parameters in Eqs. (2) and (3b) are allowed to vary to achieve the best fit shown in Fig. 2. This includes the distance between the last SiC bilayer and the graphitic interface layer D_0 and the distance between this layer and the next graphene layer D_1 that relax to best-fit values of 2.55 and 3.62 Å, respectively. Note that D_1 is larger than the bulk graphite spacing of 3.354 Å. As can be seen in Fig. 2, this model gives a very poor fit to the data at values of $\ell=5$ and 9, which are the anti-Bragg points for SiC. This is typical of all bulk-terminated models including those with a substantial modulation of the first graphene layer such as the calculated $(6\sqrt{3}\times 6\sqrt{3})$R30 surface of Varchon *et al.*[53] and Kim *et al.*[55] The calculated reflectivity from this theoretical interface, including a relaxed bulk surface and the structure factor $F_1(\ell)$ of the rippled first graphene layer, gives similarly poor fits to the reflectivity near the anti-Bragg positions.

Better fits can be obtained by an extended interface where an additional partial layer of adatoms is added to the simple relaxed bilayer model (see the schematic models in Fig. 2). As demonstrated in Fig. 2, the additional density from the adatoms begins to correct many of the deficiencies in the relaxed bulk model fit at the anti-Bragg points (especially near $\ell=9$). Note that the adatom model used to fit the reflectivity is very similar to the model proposed by Rutter *et al.*,[31] including the Si adatom density which is $\rho_{ad}=0.21$ compared to 0.22 in their model.

The improvement in the calculated intensities by adding an adatom layer is due to the increased scattered intensity at the SiC anti-Bragg condition that would be zero for a bulk terminated interface. Regardless, the simple adatom model cannot reproduce a number of features in the reflectivity data for $\ell>4$. The inability of this model to fit the experimental data is a result of both an insufficient atomic density in the interface and the atomic gradient through the interface. Increasing the width of the interface adds an additional Fourier component in Eq. (2) that both broadens the fit near $\ell\sim 6$ and removes the interference minimum at $\ell\sim 9$. Therefore, to improve the fits, it is necessary to change both the atom distribution and the thickness of the interface layer. The need for an additional plane of atoms is also consistent with number of STM experiments of the SiC(0001) $(6\sqrt{3}\times 6\sqrt{3})$R30 interface. STM images of "trimerlike" structures suggest at least one additional partial layer of atoms.[24,29–31,39]

Adding a fifth layer of atoms and changing the atom density in the interface layer-0 leads to a set of nearly identical structures that are shown in Fig. 3. These structures are distinguished by whether an atom plane in the interface is composed of either carbon or silicon atoms. This is because in x-ray diffraction the ratio of atomic form factors of Si and C used in Eq. (2) is determined, to first order, by the ratio of their atomic numbers $14/6=2.33$. Therefore, the model calculation should give a similar fit if all silicon atoms are replaced by carbon atoms with 2.33 times the density (however, there is a substantial difference in the ℓ dependence of the Si and C atomic form factors that affects both ρ's and z_j's in the final fits). While x-ray reflectivity data alone is unable to distinguish between different silicon and carbon compositions in the interface layer, spectroscopic data from a number of experimental groups place restrictions on the atomic makeup of layer-0 in Fig. 1.

Angle-resolved photoemission spectroscopy (ARPES) studies by Emtsev *et al.*[56] as well as x-ray photoemission

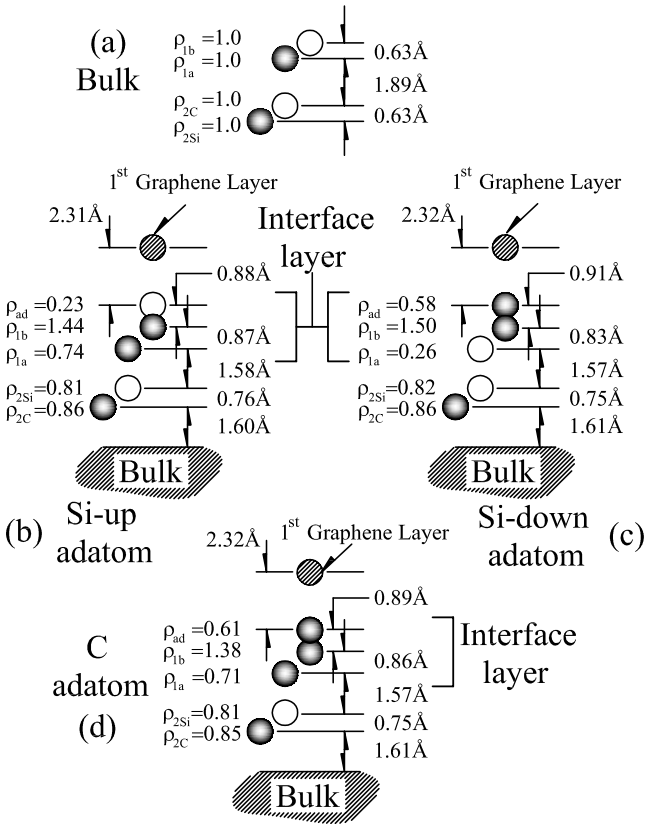

FIG. 3. Three graphene/SiC interface ball models for graphene grown on the Si face of SiC determined by surface x-ray reflectivity; (b) Si-up model, (c) Si-down model, and (d) C-adatom model. Open circles are silicon atoms and shaded circles are carbon atoms. The densities ρ are relative to the densities of bulk SiC shown in (a).

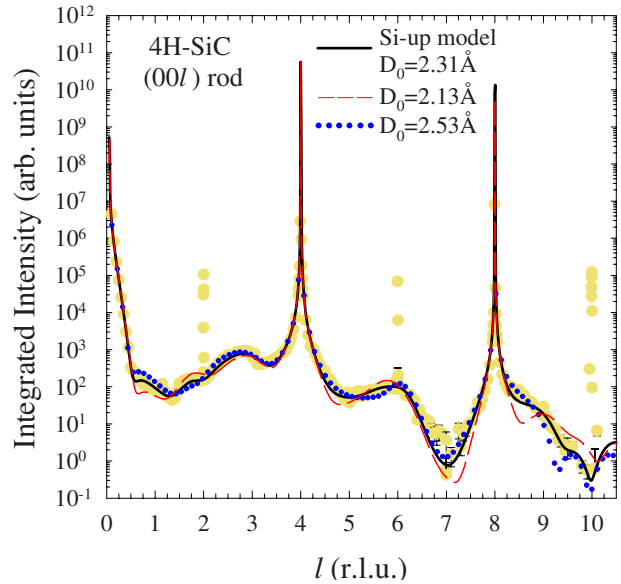

FIG. 4. (Color online) Specular reflectivity versus $q_\perp$ (in r.l.u.) for a graphitized 4H-SiC(0001) Si-face surface. Circles are the data. Solid black line is the best fit to the Si-up model in Fig. 3(b) with D_0=2.31 Å (the C-adatom and Si-down model fits would be indistinguishable). Dashed red line is the same fit but with a smaller D_0=2.13 Å. Dotted blue line is the same fit but with a larger D_0 =2.53 Å.

spectroscopy (XPS) studies by Johansson *et al.*[28] conclude that the interface layer has a significant carbon concentration (at least 1.3 times more than the carbon in a bulk SiC bilayer[28]) that rules out a purely silicon interface. In fact the x-ray diffraction also rules out a purely silicon interface because the density of silicon required to get reasonable fits to the reflectivity data is almost half the density required for an sp^3 silicon film, which is physically unreasonable. These spectroscopic constraints reduce the number of possible structures that are compatible with the reflectivity data to three, the "C-adatom," "Si-up," and "Si-down," models shown in Fig. 3.

The best reflectivity fit to the data is nearly identical for all three models and is shown in Fig. 4. Table II gives the fitting parameters for all models (uncertainty limits include variations from sample to sample). In the C-adatom model a carbon-rich layer composed of three carbon layers is sandwiched between the graphene and a distorted SiC bilayer. The total density of these three interface layers is $\rho=0.61+1.38+0.71=2.70\pm0.15$. This density is lower than the density of a graphene sheet ($\rho_G=3.13$) but is 30% higher than a bulk SiC bilayer. The two Si models are similar to the C-adatom model in that they contain a carbon-rich layer, although it is composed of two rather than three carbon layers sandwiched between the graphene. The total carbon density of the interface layers in the Si-up and Si-down models are $\rho=1.44+0.74=2.18\pm0.15$ and $0.58+1.50=2.08\pm0.15$, respectively. These values are similar to the total bulk bilayer density ($\rho=2.0$) needed to form a sp^3-bonded carbon layer. The two Si models are distinguished by a low density of Si atoms either atop or below the carbon-rich interface layer.

There are two similarities between all three models. First, the high carbon densities in all three models suggest a complicated carbon bonding geometry that is neither like bulk SiC nor like graphene. This has also been noted by both Emtsev *et al.*[54,56] and Johansson *et al.*[28] who studied the $(6\sqrt{3}\times6\sqrt{3})$R30 reconstruction that forms before graphitization and is known to persist after a true graphene layer has formed. The ARPES data of Emtsev *et al.*[54,56] show that the interface layer has σ bands (although shifted to higher energy) but no π bands. This suggests that the carbon concentration is high enough to at least locally support a sp^2 bonding geometry. In addition, the XPS studies of both Johansson *et al.*[28] and Emtsev *et al.*[56] find two surface-related C 1*s* core-level shifts. As a result both studies conclude that the $(6\sqrt{3}\times6\sqrt{3})$R30 surface contains a large amount of nongraphitic carbon in inequivalent surface sites in spite of the σ bands.

The second similarity between these models is that, unlike the SiC$(000\bar{1})$ C face,[46] the Si-face interface reconstruction extends deeper into the bulk. The bilayer between the interface layer and the bulk is substantially altered from a bulk bilayer in both density and bonding. This deep reconstruction on the (0001) surface is consistent with the prediction of Johansson *et al.*[28] based on relative intensity ratios of surface to bulk XPS peaks. Regardless of the model, the bond lengths between this bilayer and both the bulk and the inter-

TABLE II. Best-fit structural parameters for graphite-covered 4H-SiC(0001) Si face. Data for the Si-up, Si-down, and C-adatom models give nearly identical fits. Parameters are defined in Fig. 1.

	d_{ad} (Å)	ρ_{ad} (Å)	Δ_{1b} (Å)	ρ_{1b} (Å)	Δ_{1a} (Å)	ρ_{1a}	Δ_{2C} (Å)	ρ_{2C}	Δ_{2Si} (Å)	ρ_{2Si}
Si up	0.88	0.23	−0.23	1.44	−0.47	0.74	−0.29	0.86	−0.16	0.81
Atom type		silicon		carbon		carbon				
Si down	0.91	0.58	−0.28	1.50	−0.48	0.26	−0.28	0.86	−0.16	0.82
Atom type		carbon		carbon		silicon				
C-adatom	0.89	0.61	−0.25	1.38	−0.48	0.71	−0.28	0.85	−0.15	0.81
Atom type		carbon		carbon		carbon				
Uncertainty	0.04	0.08	0.04	0.08	0.04	0.1	0.05	0.1	0.05	0.08

face layer are contracted by ~17% from the bulk Si-C bond length making them similar to the bonds in diamond (1.54 Å).[57]

IV. DISCUSSION

The main difference between the C-adatom and either the Si-up or Si-down models is the low-density Si layer in the interface region. While x-ray data alone cannot discriminate between an all-carbon interface and a carbon-rich interface with silicon, spectroscopic measurements strongly favor the two models with silicon in the interface. XPS and photoemission spectroscopy (PES) experiments conclude that, after graphene has formed, a significant fraction of Si remains at the interface.[28,39,58] A complete XPS study by Johansson *et al.*[28] finds that in addition to two surface-related C 1*s* core-level shifts, there are also two surface-related Si 2*p* core-level shifts.[59] This is consistent with a Si-adatom layer in the interface and a modified Si-C bond between the interface and the bulklike bilayer below. We note that the bonding configuration of the Si-up model is very similar to a model proposed from STM images of the $(6\sqrt{3}\times 6\sqrt{3})$R30 interface structure below a layer of graphene.[31] The model of Rutter *et al.*[31] suggests an adatom density of $\rho_{ad}=0.22$, which is within error bars of the x-ray value in Table II. At the moment, however, there are no experimental data that can exclude either of the two Si models.

It is worth pointing out a number of important structural differences between Si-face-grown graphene and C-face-grown graphene. Table III shows a comparison of structural parameters determined from x-ray reflectivity data for graphene grown on the SiC(0001) and SiC(000$\bar{1}$) surfaces. The distance between the first graphene layer and the interface for Si-face graphene film is $D_0=2.3\pm 0.08$ Å. Figure 4 shows the sensitivity of the fit to either increasing or decreasing the value of D_0 by 9%. The measured value of D_0 is large compared to the bilayer distance in bulk SiC (1.89 Å) and at the same time less than the graphite interplanar spacing of 3.354 Å.[45] Note that the best-fit value of D_0 is similar to the value of 2.5 Å measured by STM.[31] The Si-face value of D_0 is larger than the value for furnace grown graphene on the SiC(000$\bar{1}$) C face, implying that graphene is more strongly bound to the C-face interface. This is consistent with *ab initio* electronic calculations[41,42] and the conclusions of previous inverse photoemission, PES, and XPS studies[13,14,60] (recent ARPES experiments have a contradictory interpretation to these studies, suggesting that the C-face graphene grown in UHV is in fact less tightly bound to the interface compared to the Si face[54]). It is also worth pointing out that Table III compares Si-face graphene to C-face graphene grown in a furnace; UHV C-face graphene used in previous studies[13,14,54] grows nearly 200 °C lower in UHV compared to graphene grown in a furnace.[15] This temperature difference may influence the interface structure or order and should be considered when comparing results from different groups.

In addition to D_0, Table III also shows that the spacing D_1 between graphene layer-1 and layer-2 is larger than the spacing between all other graphene layers (for both Si-face and C-face graphenes). Note that the error bar on D_G is significantly larger than those reported for C-face graphene films. This is because furnace-grown C-face graphene films are much thicker than UHV-grown Si-face films. Thinner films broaden the graphene Bragg peaks at $\ell=3$, 6, and 9, making the peak position and thus the layer spacing more difficult to measure. Table III also shows that the roughness of the SiC surface is more than an order of magnitude larger for Si-face graphene than for C-face graphene (the surface roughness is

TABLE III. Structural parameters for graphene grown in UHV on 4H-SiC(0001) Si face (determined from this work) and those from furnace-grown 4H-SiC(000$\bar{1}$) C-face graphene measured in Ref. 46. Parameters are defined in Fig. 1.

	D_0 (Å)	D_1 (Å)	D_G (Å)	σ_G (Å)	γ_{SiC}
Si Face	2.32 ± 0.08	3.50 ± 0.05	3.35 ± 0.01	0.16(−0.05/+0.02)	0.7 ± 0.1
C face	1.62 ± 0.08	3.41 ± 0.04	3.368 ± 0.005	<0.05	0.03 ± 0.01

proportional to γ_{SiC}). This is consistent with earlier x-ray results[5] measuring growth-induced substrate roughness and with the substrate roughness observed in many STM and AFM images.[4,30,35,61]

The most important result of this work is that the interface layer for Si-face graphene is not a simple relaxed bulk termination of the SiC surface. This has a bearing on how to interpret electronic structure calculations of the graphene-SiC interface. To date, *ab initio* electronic structure calculations of the graphene/SiC(0001) system have started from a flat graphene layer placed above an idealized bulk-terminated SiC surface that is allowed to relax into a slightly distorted bilayer.[31,41,42] These calculations use an artificially contracted graphene sheet that is commensurate with a small SiC cell to allow for reasonably fast calculation times. Rutter *et al.*[31] looked at a Si-adatom model but, as with other calculations, used a simple relaxed bulk SiC bilayer below the adatoms. The result of all these calculations is that the first graphene layer above the relaxed bulk SiC bilayer acts as buffer that partially isolates the electronic properties of the next graphene layer from the substrate.[41,42] While these calculations are an important first step in predicting the existence of a buffer layer, their ability to predict the structure of the interface and thus its electronic properties is a concern given that the x-ray results show a much more substantial reconstruction that has few characteristics of a bulk SiC bilayer. Further experimental evidence for a buffer layer comes from ARPES, where a carbon-rich layer with substantial sp^2 bonding is found without any indication of π-band characteristics of graphene.[28,56] ARPES measurements also clearly show π-bonded graphene layers above this carbon-rich layer, although there are different interpretations of spectral structure very close to the K point of the graphene Brillouin zone for the first of these structural graphene layers.[62,63] We suggest that in the *ab initio* results, the first graphene layer in the calculation mimics, to some extent, the properties of the interface layer-0. In fact recent *ab initio* calculations, using a full $(6\sqrt{3}\times 6\sqrt{3})$R30 cell, find that the first graphene layer is significantly distorted from a flat graphene sheet and does not show the dispersion characteristic of an isolated graphene sheet.[53,55] In fact the calculated modulation amplitude is 1.23 Å, a value not far from the ~1.8 Å interface layer width measured for all the structural models in Fig. 3. These results suggest that the assumption of a distorted thick carbon-rich layer acting like a buffer layer may be correct. A more realistic interface calculation will be necessary to test this assertion.

In addition to the interface structure, the reflectivity data provide additional evidence supporting conclusions based on STM and LEED that the $(6\sqrt{3}\times 6\sqrt{3})$R30 reconstruction observed after graphitization is a true reconstruction of the graphene film. Since the discovery of the $(6\sqrt{3}\times 6\sqrt{3})$R30 LEED pattern, it has been suggested that it is a moiré pattern due to the near commensuration of graphene with SiC.[10,25,26] Early STM experiments supported this claim because they imaged a 6×6 reconstruction[24–26,58,64] instead of the $(6\sqrt{3}\times 6\sqrt{3})$R30 pattern observed in LEED. More recent STM experiments, on the other hand, have directly imaged the $(6\sqrt{3}\times 6\sqrt{3})$R30 structure and shown that the graphene has a vertical modulation with this lateral periodicity.[30,31] Recent

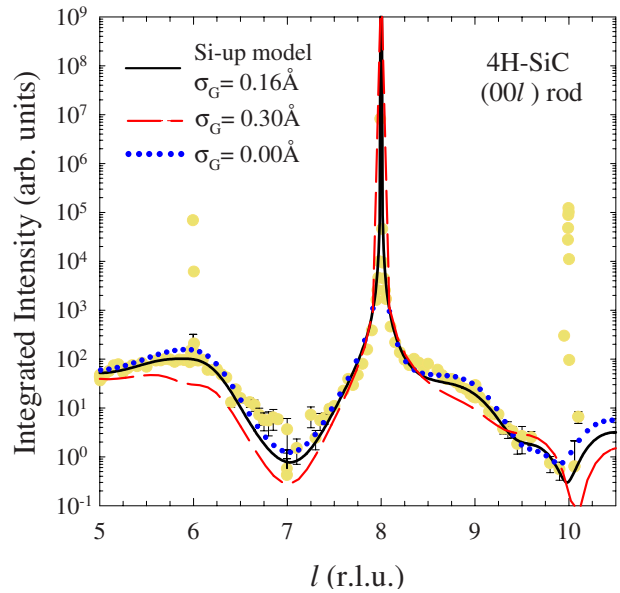

FIG. 5. (Color online) Specular reflectivity versus $q_\perp$ (in r.l.u.) for a graphitized 4H-SiC(0001) Si-face surface. Circles are the data. Solid black line is the best fit to the Si-up model with σ_G =0.16 Å. Dashed red line is the same fit but with σ_G=0.30 Å. Dotted blue line is the same fit but with a larger σ_G=0.0 Å.

ab initio calculations, using a full $(6\sqrt{3}\times 6\sqrt{3})$R30 cell, find that at least the first graphene layer above the SiC has a substantial modulation amplitude.[53] The x-ray reflectivity data support these recent experiments and confirm that there is a vertical modulation of graphene grown on the Si face. This can be seen by comparing the C-face and Si-face graphene layer roughness or corrugation σ_G from Eq. (3) (see Table III). σ_G is much larger on Si-face-grown graphene than on C-face-furnace-grown graphene. σ_G is determined almost solely by the intensity decay of the graphite Bragg points as a function of ℓ. Because of the exponential form in Eq. (3), a finite σ_G manifests itself as a decay in the graphite Bragg-peak intensities at ℓ=6 and 9. This is demonstrated in Fig. 5 where we compare fits from a graphene film with no roughness (σ_G=0 Å) to a fit with a large roughness (σ_G =0.3 Å) and to the best-fit value for the Si-up mode in these experiments σ_G=0.16 Å. Note in Table III that σ_G is essentially zero for C-face graphene films that show no LEED reconstruction patterns.[5,10,13,14] We can interpret σ_G as originating from an actual modulation of the graphene film, but the value of 0.16 Å is considerably smaller than the value of 0.6 Å measured by STM for the first graphene sheet above the interface layer.[31] This difference arises in part because STM is measuring a modulation in the electron density of states instead of an actual structural modulation and more importantly because the x-ray value is an average over all the graphene layers in the film. Riedl *et al.*[30] showed that the vertical modulation amplitude decays by approximately a factor of 2 from the first to the second graphene layer. Therefore, thicker graphene films weight the average σ_G to lower values.

We can estimate the first graphene layer modulation $\sigma_G^{(0)}$ from the measured mean modulation σ_G if we assume that the modulation decays in subsequent layers as $\sigma_G^{(n)}$

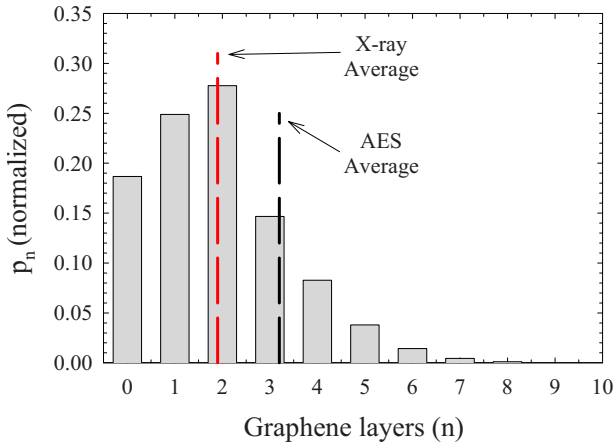

FIG. 6. (Color online) The normalized probability p_n of a n-graphene layer stack from a UHV-grown Si-face film as determined by x-ray reflectivity. The x-ray average is 1.9 ± 1.5 graphene layers while the AES estimate of the average is approximately one layer thicker (3.2 layers).

$=\sigma_G^{(0)} \exp[-\lambda Dn]$, where $\lambda D = \ln(2)$ [the factor of ln(2) assumes that the amplitude decay measured by Riedl *et al.*[30] is correct]. To calculate $\sigma_G^{(0)}$ we only need to know the relative amount of graphene that is thicker than N layers P_N. P_N is calculated from the areal coverage p_n's in Eq. (3a); $P_N = C\sum_{n=N}^{N_{max}} p_n$ (C is a normalization constant). Then $\sigma_G^{(0)}$ is given by

$$\sigma_G^{(0)} = \sigma_G \sum_n P_n / \sum_n P_n \exp[-\lambda Dn]. \quad (4)$$

The measured distribution of graphene layer thickness p_n for a nominally two-layer graphene film is shown in the layer height histogram in Fig. 6. The average number of graphene layers is 1.9 ± 1.5. The distribution is very wide, in part reflecting the spatial average over the large x-ray beam footprint (the footprint is bigger than the sample width of 3 mm when $\ell < 1.8$). In particular the high areal fraction not covered by graphene (18%) can be associated with slow growth kinetics at cooler substrate regions near the edge of the sample caused by nonuniformity in the e-beam heating. These wide distributions are also seen in low-energy electron microscope (LEEM) images.[36,37] Using this measured distribution, we estimate $\sigma_G^{(0)}$ to a range between 0.5 and 0.8 Å reflecting the uncertainty in the measured value of σ_G. This result is in very good agreement with the STM value of ~0.6 Å.[31]

For comparison, we can estimate the vertical modulation of the first graphene layer using a different method. This is done by using a modulated first graphene layer on top of the Si-up adatom model to calculate $F_1(\ell)$ in Eq. (3). To do this we use the graphene structural coordinates calculated by Varchon *et al.*[53] The modulation of higher graphene layers are included using the rms roughness in the standard model. While the calculated relative vertical carbon positions are maintained in the first graphene layer, the absolute positions are scaled by a multiplicative constant so that the peak-to-peak amplitude can be varied. The best-fit structure to the reflectivity data gives the first graphene layer amplitude to be 0.82 Å peak to peak, which is slightly larger than the range of $\sigma_G^{(0)}$ estimated above.

It is worth comparing the graphene thickness measured by surface x-ray diffraction and an estimate from the simpler AES method.[11,65,66] The ratio of the Si(LVV)/C(KLL) peak area can be used, along with proper electron mean-free paths and excitation cross sections, to estimate of the number of graphene layers provided that a suitable model for the interface is used. Most groups use an interface model consisting of a bulk-terminated substrate with graphene above.[11,65] (Ref. 66 considers a $\sqrt{3} \times \sqrt{3}$ Si adlayer.) While bulk termination is clearly inconsistent with both models in Fig. 3, it can still be used with the proviso that it will overestimate the film thickness by ~1 layer because the measured C(KLL) intensity includes a contribution from the dense nongraphitic interface carbon layer in Fig. 3. AES measurements on the same sample as the data for Fig. 6 estimate the average graphene coverage to be 3.2 layers compared to 1.9 by x rays, consistent with the lack of a realistic interface layer in the AES calculation. Because the electron penetration depth of the Si(LVV) electron is short, AES estimates become more uncertain for graphene layers exceeding four layers. This makes the AES method more applicable to Si-face films than to thick-furnace-grown C-face graphene films.

V. CONCLUSION

We have used surface x-ray reflectivity measurements to determine the graphene/SiC interface structure for graphene grown on the 4H-SiC(0001) Si-terminated surface (Si-face). We find that the interface is not composed of a simple graphene-like layer above a relaxed SiC bilayer that has been recently proposed.[54] Instead, the interface reconstruction is more complicated and extends deeper into the bulk. Based on these x-ray experiments and previous XPS studies[28] the best model for the interface is composed of a substantially relaxed SiC bilayer, above which a dense carbon layer containing a partial layer of Si atoms separates it from the graphene film. The carbon density in this intermediate layer is approximately 2.1 times larger than in a SiC bilayer. This model is consistent with previous STM (Refs. 24, 30, and 31) and XPS (Ref. 28) results as well as the lack of interface π bands in ARPES experiments.[54,56] The bond distance between the Si adatom layer and the first graphene layer (Si-up model) is 2.32 ± 0.08 Å. While this distance is short compared to the interplanar graphene spacing, it is still larger than the corresponding distance measured on furnace-grown SiC($000\bar{1}$) C-face graphene (1.62 Å),[46] indicating that the graphene on the Si-face is less tightly bounded to the substrate than furnace-grown C-face graphene. This difference is consistent with *ab initio* calculations.[41] We propose that the dense carbon layer with Si adatoms plays the role of the buffer layer predicted by Varchon *et al.*[41] It is this layer that partly isolates subsequent graphene layers from interactions with the substrate.

The x-ray results also indicate that the graphene is not flat but has a corrugation amplitude between 0.5 and 0.8 Å. This is consistent with the 0.6 Å corrugation amplitude of the

(6×6) reconstruction measured by STM.[30,31] Because measured STM corrugations can be due to changes in the local density of states, the similarity between the STM and x-ray corrugation values confirms that the reconstruction imaged by STM is dominated by a real structural corrugation of the graphene.

ACKNOWLEDGMENTS

We wish to thank I. Gadjev and K. Charulatha for helping us to prepare the reflectivity data and fits. We also would like to thank C. Berger and W. A. de Heer for helpful discussions and F. Varchon and L. Magaud for providing the atomic coordinates from their graphene/SiC interface calculations. This research was supported by the National Science Foundation under Grant Nos. 0404084 and 0521041, by the Intel Research, and by the W. M. Keck Foundation. The Advanced Photon Source is supported by the DOE Office of Basic Energy Sciences under Contract No. W-31-109-Eng-38. The μ-CAT beam line is supported through Ames Laboratory operated for the U.S. DOE by Iowa State University under Contract No.W-7405-Eng-82.

[1] International Technology Roadmap for Semiconductors Emerging Research Materials, 2007 (unpublished), p. 5.
[2] C. Berger, Z. Song, T. Li, X. Li, A. Y. Ogbazghi, R. Feng, Z. Dai, A. N. Marchenkov, E. H. Conrad, P. N. First, and W. A. de Heer, J. Phys. Chem. B **108**, 19912 (2004).
[3] C. Berger, Z. Song, X. Li, X. Wu, N. Brown, C. Naud, D. Mayou, T. Li, J. Hass, A. N. Marchenkov, E. H. Conrad, P. N. First, and W. A. de Heer, Science **312**, 1191 (2006).
[4] W. A. de Heer, C. Berger, X. Wu, P. N. First, E. H. Conrad, X. Li, T. Li, M. Sprinkle, J. Hass, M. L. Sadowski, M. Potemski, and G. Martinez, Solid State Commun. **143**, 92 (2007).
[5] J. Hass, R. Feng, T. Li, X. Li, Z. Song, W. A. de Heer, P. N. First, E. H. Conrad, C. A. Jeffrey, and C. Berger, Appl. Phys. Lett. **89**, 143106 (2006).
[6] J. Kedzierski, P.-L. Hsu, P. Healey, P. Wyatt, C. Keast, M. Sprinkle, C. Berger, and W. de Heer, IEEE Trans. Electron Devices **55**, 2078 (2008).
[7] M. L. Sadowski, G. Martinez, M. Potemski, C. Berger, and W. A. de Heer, Phys. Rev. Lett. **97**, 266405 (2006).
[8] M. L. Sadowski, G. Martinez, M. Potemski, C. Berger, and W. A. de Heer, Solid State Commun. **143**, 123 (2007).
[9] X. Wu, X. Li, Z. Song, C. Berger, and W. A. de Heer, Phys. Rev. Lett. **98**, 136801 (2007).
[10] A. J. Van Bommel, J. E. Crombeen, and A. Van Tooren, Surf. Sci. **48**, 463 (1975).
[11] L. Muehlhoff, W. J. Choyke, M. J. Bozack, and J. T. Yates, J. Appl. Phys. **60**, 2842 (1986).
[12] I. Forbeaux, J.-M. Themlin, and J.-M. Debever, Phys. Rev. B **58**, 16396 (1998).
[13] I. Forbeaux, J.-M. Themlin, and J.-M. Debever, Surf. Sci. **442**, 9 (1999).
[14] I. Forbeaux, J.-M. Themlin, A. Charrier, F. Thibaudau, and J.-M. Debever, Appl. Surf. Sci. **162-163**, 406 (2000).
[15] J. Hass, W. A. de Heer, and E. H. Conrad, J. Phys.: Condens. Matter **20**, 323202 (2008).
[16] F. Varchon, P. Mallet, L. Magaud, and J.-Y. Veuillen, Phys. Rev. B **77**, 165415 (2008).
[17] K. V. Emtsev, A. Bostwick, K. Horn, J. Jobst, G. L. Kellogg, L. Ley, J. L. McChesney, T. Ohta, S. A. Reshanov, E. Rotenberg, A. K. Schmid, D. Waldmann, H. B. Weber, and T. Seyller, arXiv:0808.1222 (unpublished).
[18] M. Orlita, C. Faugeras, P. Plochocka, P. Neugebauer, G. Martinez, D. K. Maude, A.-L. Barra, M. Sprinkle, C. Berger, W. A. de Heer, and M. Potemski, arXiv:0808.3662 (unpublished).
[19] T. Ohta, A. Bostwick, J. L. McChesney, T. Seyller, K. Horn, and E. Rotenberg, Phys. Rev. Lett. **98**, 206802 (2007).
[20] J. Hass, F. Varchon, J. E. Millan-Otoya, M. Sprinkle, N. Sharma, W. A. de Heer, C. Berger, P. N. First, L. Magaud, and E. H. Conrad, Phys. Rev. Lett. **100**, 125504 (2008).
[21] M. Naitoh, M. Kitada, S. Nishigaki, N. Toyama, and F. Shoji, Surf. Rev. Lett. **10**, 473 (2003).
[22] J. M. B. Lopes dos Santos, N. M. R. Peres, and A. H. Castro Neto, Phys. Rev. Lett. **99**, 256802 (2007).
[23] S. Latil, V. Meunier, and L. Henrard, Phys. Rev. B **76**, 201402(R) (2007).
[24] F. Owman and P. Mårtensson, Surf. Sci. **330**, L639 (1995).
[25] C. S. Chang, I. S. T. Tsong, Y. C. Wang, and R. F. Davis, Surf. Sci. **256**, 354 (1991).
[26] L. Li and I. S. T. Tsong, Surf. Sci. **351**, 141 (1996).
[27] A. Charrier, A. Coati, T. Argunova, F. Thibaudau, Y. Garreau, R. Pinchaux, I. Forbeaux, J.-M. Debever, M. Sauvage-Simkin, and J.-M. Themlin, J. Appl. Phys. **92**, 2479 (2002).
[28] L. I. Johansson, F. Owman, and P. Mårtensson, Phys. Rev. B **53**, 13793 (1996).
[29] V. W. Brar, Y. Zhang, Y. Yayon, T. Ohta, J. L. McChesney, A. Bostwick, E. Rotenberg, K. Horn, and M. F. Crommie, Appl. Phys. Lett. **91**, 122102 (2007).
[30] C. Riedl, U. Starke, J. Bernhardt, M. Franke, and K. Heinz, Phys. Rev. B **76**, 245406 (2007).
[31] G. M. Rutter, N. P. Guisinger, J. N. Crain, E. A. A. Jarvis, M. D. Stiles, T. Li, P. N. First, and J. A. Stroscio, Phys. Rev. B **76**, 235416 (2007).
[32] T. Ohta, A. Bostwick, T. Seller, K. Horn, and E. Rotenberg, Science **313**, 951 (2006).
[33] E. Rollings, G.-H. Gweon, S. Y. Zhou, B. S. Mun, J. L. McChesney, B. S. Hussain, A. V. Fedorov, P. N. First, W. A. de Heer, and A. Lanzara, J. Phys. Chem. Solids **67**, 2172 (2006).
[34] G. M. Rutter, J. N. Crain, N. P. Guisinger, T. Li, P. N. First, and J. A. Stroscio, Science **317**, 219 (2007).
[35] Th. Seyller, K. V. Emtsev, K. Gao, F. Speck, L. Ley, A. Tadich, L. Broekman, J. D. Riley, R. C. G. Leckey, O. Rader, A. Varykhalov, and A. M. Shikin, Surf. Sci. **600**, 3906 (2006).
[36] H. Hibino, H. Kagashima, F. Maeda, M. Nagase, Y. Kobayashi, and H. Yamaguchi, Phys. Rev. B **77**, 075413 (2008).
[37] T. Ohta, F. El Gabaly, A. Bostwick, J. McChesney, K. V. Emtsev, A. K. Schmid, T. Seyller, K. Horn, and E. Rotenberg, New J. Phys. **10**, 023034 (2008).
[38] P. Lauffer, K. V. Emtsev, R. Graupner, T. Seyller, L. Ley, S. A.

Reshanov, and H. B. Weber, Phys. Rev. B **77**, 155426 (2008).
[39] W. J. Ong and E. S. Tok, Phys. Rev. B **73**, 045330 (2006).
[40] P. Mallet, F. Varchon, C. Naud, L. Magaud, C. Berger, and J.-Y. Veuillen, Phys. Rev. B **76**, 041403(R) (2007).
[41] F. Varchon, R. Feng, J. Hass, X. Li, B. N. Nguyen, C. Naud, P. Mallet, J. Y. Veuillen, C. Berger, E. H. Conrad, and L. Magaud, Phys. Rev. Lett. **99**, 126805 (2007).
[42] A. Mattausch and O. Pankratov, Phys. Rev. Lett. **99**, 076802 (2007).
[43] Cree Inc., 4600 Silicon Drive, Durham, NC 27703.
[44] A. Bauer, J. Kräusslich, L. Dressler, P. Kuschnerus, J. Wolf, K. Goetz, P. Käckell, J. Furthmüller, and F. Bechstedt, Phys. Rev. B **57**, 2647 (1998).
[45] Y. Baskin and L. Mayer, Phys. Rev. **100**, 544 (1955).
[46] J. Hass, R. Feng, J. E. Millán-Otoya, X. Li, M. Sprinkle, P. N. First, W. A. de Heer, E. H. Conrad, and C. Berger, Phys. Rev. B **75**, 214109 (2007).
[47] I. K. Robinson, in *Handbook on Synchrotron Radiation*, edited by G. S. Brown and D. E. Moncton (North-Holland, Amsterdam, 1991), Vol. 3, p. 221.
[48] E. Vlieg, J. Appl. Crystallogr. **30**, 532 (1997).
[49] R. Feng, Ph.D. thesis, Georgia Institute of Technology, 2006.
[50] W. C. Elliott, P. F. Miceli, T. Tse, and P. W. Stephens, Physica B **221**, 65 (1996).
[51] A. Bauer, Ph. Reischauer, J. Kräusslich, N. Schell, W. Matz, and K. Goetz, Acta Crystallogr., Sect. A: Found. Crystallogr. **57**, 60 (2001).
[52] I. K. Robinson, Phys. Rev. B **33**, 3830 (1986).
[53] F. Varchon, P. Mallet, J.-Y. Veuillen, and L. Magaud, Phys. Rev. B **77**, 235412 (2008).
[54] K. V. Emtsev, F. Speck, Th. Seyller, L. Ley, and J. D. Riley, Phys. Rev. B **77**, 155303 (2008).
[55] S. Kim, J. Ihm, H. J. Choi, and Y. W. Son, Phys. Rev. Lett. **100**, 176802 (2008).
[56] K. V. Emtsev, T. Seyller, F. Speck, L. Ley, P. Stojanov, J. D. Riley, and R. G. C. Leckey, Mater. Sci. Forum **556-557**, 525 (2007).
[57] J. K. Burdett, *Chemical Bonding in Solids* (Oxford University Press, New York, 1995), p. 152.
[58] W. Chen, H. Xu, L. Liu, X. Gao, D. Qi, G. Peng, S. C. Tan, Y. Feng, K. P. Loh, and A. T. S. Wee, Surf. Sci. **596**, 176 (2005).
[59] Emtsev *et al.* (Ref. 56) also carried out XPS measurements on this surface, but they suggest that the $6\sqrt{3}$ interface is all carbon. However, they have not published Si $2p$ core-level spectra to confirm this assertion.
[60] L. I. Johansson, P.-A. Glansm, and N. Hellgren, Surf. Sci. **405**, 288 (1998).
[61] G. Gu, S. Nie, R. M. Feenstra, R. P. Devaty, W. J. Choyke, W. K. Chan, and M. G. Kane, Appl. Phys. Lett. **90**, 253507 (2007).
[62] A. Bostwick, T. Ohta, T. Seyller, K. Horn, and E. Rotenberg, Nat. Phys. **3**, 36 (2007).
[63] S. Y. Zhou, G.-H. Gweon, A. V. Fedorov, P. N. First, W. A. De Heer, D.-H. Lee, F. Guinea, A. H. Castro Neto, and A. Lanzara, Nature Mater. **6**, 770 (2007).
[64] T. Tsukamoto, M. Hiria, M. Kusaka, M. Iwami, T. Ozawa, T. Nagamura, and T. Nakata, Appl. Surf. Sci. **113-114**, 467 (1997).
[65] T. Tsukamoto, M. Hiria, M. Kusaka, M. Iwami, T. Ozawa, T. Nagamura, and T. Nakata, Surf. Sci. **371**, 316 (1997).
[66] T. Li, Ph.D. thesis, Georgia Institute of Technology, 2006.